Optimal Ship-to-Grid Dispatch Considering Battery Thermal and Voltage Electrochemical-Thermal-Coupled Constraints

Chao Lei, *Member, IEEE*, Shuangqi Li, *Member, IEEE*, and Yu Christine Chen, *Member, IEEE*

***Abstract*—This letter proposes an optimal ship-to-grid (S2G) dispatch model of electric ships (ESs) coupling onshore and/or offshore wind energy conversion systems (WECS) with shore-to-ship and/or offshore floating charging stations so that the shipboard battery energy storage system (BESS) can help to smooth out variable WECS output. Thermal and voltage constraints of battery cells based on the electrochemical-thermal-coupled model enable fast charging to full capacity in the constant-current (CC) charging mode while remaining within battery operational limits. Case studies demonstrate that the proposed optimal S2G dispatch solution is physically realizable and fully satisfies the battery charging needs of ESs within thermal security constraints.**

***Index Terms*—Battery, electrochemical, optimal battery dispatch, ship-to-grid dispatch, thermal, voltage**

I. Introduction

DECARBONIZATION of marine transport has motivated the adoption of electric ships (ESs) that can greatly reduce emissions if the shipboard battery energy storage system (BESS) charges using clean electricity sources, such as onshore or offshore wind energy conversion systems (WECS) [1]. Conversely, the shipboard BESS can provide key grid service, e.g., smoothing out variable WECS output, via ship-to-grid (S2G) dispatch (see Fig. 1) [2].

The BESS in an ES is generally configured with many battery modules, each containing several battery cells. If ESs need to charge or discharge power at high rates possible with rapid fluctuations in WECS outputs, battery cell temperatures can exceed the range considered to be safe, leading to potential disconnection of the cells [3]. Thus, thermal constraints of battery cells are important to consider for use with WECS. Another important consideration is cell voltage. A battery cell typically charges in constant-current (CC) mode with a prescribed current before reaching its maximum allowable voltage limit, then charging shifts to constant-current-constant-voltage (CCCV) mode that gradually reduces current until the cell becomes fully charged [4]. However, lowering the charging rate as the battery cell nears full capacity may not smooth out WECS outputs as intended, yet charging the cell to full capacity at a high current in the CC mode becomes impossible once the maximum allowable voltage is reached [4]. However, charging a BESS to full capacity is essential to maximize the potential for ESs to serve as long-voyage transport, especially with limited access to offshore charging infrastructure. It is worth noting that charging to full capacity does not itself accelerate battery degradation so long as the depth of discharging is kept within reasonable range in the case that charging infrastructure is not limited [5].

Chao Lei and Yu Christine Chen are with the Department of Electrical and Computer Engineering, The University of British Columbia, Vancouver, Canada. E-mail: chaolei@ece.ubc.ca and chen@ece.ubc.ca. Shuangqi Li is with the Department of Electrical and Electronic Engineering, Hong Kong Polytechnic University, Hong Kong, China. E-mail: shuangqi.li@polyu.edu.hk. This work was supported by the Natural Sciences and Engineering Research Council of Canada (NSERC), funding reference number 554474-2020.

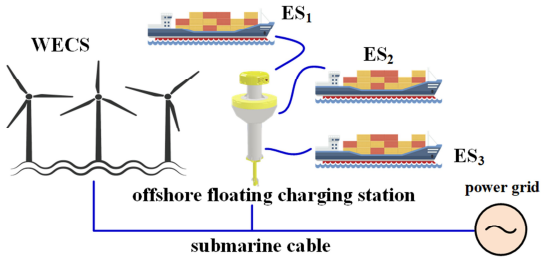

Fig. 1. Illustrating the proposed ship-to-grid dispatch architecture: BESSs in ESs offer grid services, such as smoothing out variable WECS output.

To address the aforementioned challenges, this letter develops an optimal S2G dispatch model for ESs that accounts for temperature variations and voltage characteristics of battery cells based on the electrochemical-thermal-coupled model. Related work in this domain includes [6] that approximates cell temperature variations using a lumped estimation method considering only the initial cell temperature and charge/discharge rate but not the dependence on the cell's state of charge (SoC), which may result in suboptimal or even infeasible battery dispatch. For voltage constraints of battery cells considered in [7], polarization effects are not modelled for the CC charging mode. Thus the approximation of voltage variations may not apply to battery charging close to full capacity, especially for ES's battery energy storage systems (BESSs) with $LiFePO_4$ (LFP) electrodes more sensitive to polarization at higher currents [8]. Also, related work in electric vehicles (EVs) generally focuses on a single EV charging with battery cell thermal or voltage constraints instead of addressing optimal operation involving fleets of EVs [9]. Our approach advances the state-of-the-art in optimal battery dispatch (see, e.g., [10]) by incorporating more practical battery models accounting for cell thermal and voltage constraints into an optimal S2G dispatch problem.

II. Optimal S2G Dispatch

A. Thermal Constraints of Battery Cells

Consider a scheduling horizon subdivided into time periods of length $\Delta t\,[\mathrm{min}]$ (e.g., 15 minutes) collected in the set $\mathcal{T} = \{0, \Delta t, 2\Delta t, \ldots, N_T \Delta t\}$. Denote by $T_i^t\,[\mathrm{K}]$ the average cell temperature for a battery cell in the BESS in ES_i in time period $t \in \mathcal{T}$. We adopt a lumped heat model consisting of a single uniform temperature across the entire cell, as follows: [6]

$$m_i C_{p,i} \frac{\mathrm{d}T_i^t}{\mathrm{d}t} = H_{e,i}^t + h_{c,i} A_{\mathrm{s},i} (T_{\mathrm{amb}} - T_i^t), \qquad (1)$$

where $m_i\,[\mathrm{kg}]$ denotes the mass of each battery cell, $C_{p,i}\,[\mathrm{J}/(\mathrm{kg}\cdot\mathrm{K})]$ its heat capacity, $h_{c,i}\,[\mathrm{W}/(\mathrm{m}^2\cdot\mathrm{K})]$ its heat

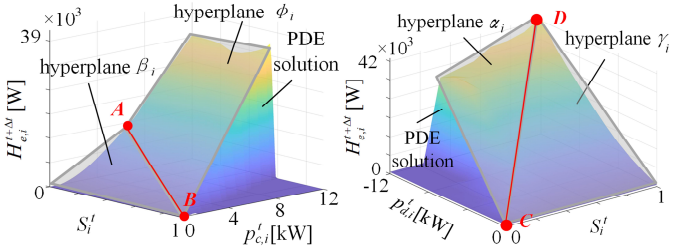

Fig. 2. Approximating $H_{e,i}^{t+\Delta t}$ for battery cell (a) charging, (b) discharging.

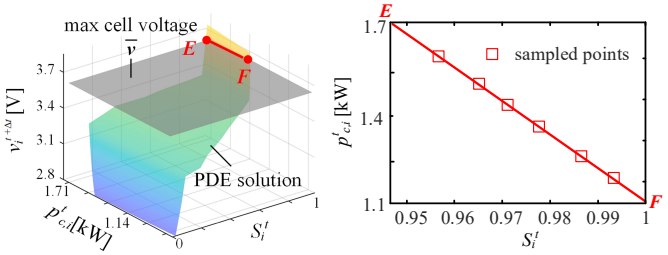

Fig. 3. Cell voltage profile (a) surface, (b) projection at upper voltage limit.

transfer coefficient, $A_{s,i}$ [m^2] its surface area, and T_{amb} [K] the ambient temperature. Also in (1), $H_{e,i}^t$ [W] denotes the heat produced in electrochemical energy conversion of a battery cell, which can be obtained at the end of time period $t \in \mathcal{T}$ from a partial differential equation (PDE) solution of the electrochemical-thermal-coupled model to inform the effect of temperature on electrochemical processes and vice versa [9].

We discretize continuous-time dynamics in (1) using the modified Euler method, with n (e.g., 10) equal discretization segments of length Δh [sec] (e.g., 90 [sec]) subdividing each time period of length Δt, as follows:

$$\widehat{T}_{i,j+1}^t = T_{i,j}^t + \Delta h \frac{\mathrm{d}T_{i,j}^t}{\mathrm{d}t}, \ j = 0, 1, \ldots, n-1, \tag{2}$$

where $\Delta h = \Delta t/n$, the result of which is substituted into

$$T_{i,j+1}^t = T_{i,j}^t + \frac{\Delta h}{2}\Big(\frac{\mathrm{d}T_{i,j}^t}{\mathrm{d}t}\Big|_{T_{i,j}^t = T_{i,j}^t} + \frac{\mathrm{d}T_{i,j}^t}{\mathrm{d}t}\Big|_{T_{i,j}^t = \widehat{T}_{i,j+1}^t}\Big). \tag{3}$$

Given boundary conditions $T_i^t = T_{i,0}^t$ and $T_i^{t+\Delta t} = T_{i,n}^t$, we can evaluate $T_i^{t+\Delta t}$ in closed form as follows: [11]

$$T_i^{t+\Delta t} = \omega_1^n T_i^t + \frac{1-\omega_1^{n-1}}{1-\omega_1}\Big(\omega_2 H_{e,i}^{t+\Delta t} + \omega_3\Big), \tag{4a}$$

$$\omega_1 = 1 - \frac{h_{c,i}A_{s,i}\Delta h}{2m_i C_{p,i}}\Big(2 - \frac{h_{c,i}A_{s,i}\Delta h}{m_i C_{p,i}}\Big), \tag{4b}$$

$$\omega_2 = \frac{\epsilon \Delta h}{m_i C_{p,i}} - \frac{\epsilon h_{c,i}A_{s,i}\Delta h^2}{2m_i^2 C_{p,i}^2}, \tag{4c}$$

$$\omega_3 = \frac{T_{\mathrm{amb}} h_{c,i}A_{s,i}\Delta h}{m_i C_{p,i}} - \frac{T_{\mathrm{amb}} h_{c,i}^2 A_{s,i}^2 \Delta h^2}{2m_i^2 C_{p,i}^2}, \tag{4d}$$

$$T_i^t \leqslant \overline{T}, \quad \forall\, t \in \mathcal{T}, \tag{4e}$$

where ϵ is a constant coefficient and $\overline{T}$ denotes the maximum cell temperature limit. Unlike [6] that accounts for the dependence of cell temperature on charging and discharging powers only, our approach more accurately models the temperature by incorporating the effects of the cell SoC, as outlined next.

A numerical PDE solution of the electrochemical-thermal-coupled model [9] yields the value of $H_{e,i}^{t+\Delta t}$ needed in (4a). We report on one such simulation over time period $\Delta t = 15$ minutes under fixed $T_{\mathrm{amb}} = 27°\mathrm{C} = 300.5\,\mathrm{K}$ and other battery parameter values reported in [11]. Fig. 2(a) (Fig. 2(b)) plots variations in $H_{e,i}^{t+\Delta t}$ with respect to SoC S_i^t and charging power $p_{c,i}^t$ (discharging power $p_{d,i}^t$). The Big-M method yields hyperplanes ϕ_i, β_i, γ_i and α_i that approximate the surfaces in Fig. 2, along with binary variables $\lambda_{\beta,i}^t$, $\lambda_{\phi,i}^t$, $\lambda_{\gamma,i}^t$, and $\lambda_{\alpha,i}^t$ to indicate where the hyperplanes are active, expressed as

$$|H_{e,i}^t - \Theta_{\beta,i}| \leqslant (2 - \lambda_{c,i}^t - \lambda_{\beta,i}^t)M, \tag{5a}$$

$$|H_{e,i}^t - \Theta_{\phi,i}| \leqslant (2 - \lambda_{c,i}^t - \lambda_{\phi,i}^t)M, \tag{5b}$$

$$|H_{e,i}^t - \Theta_{\gamma,i}| \leqslant (2 - \lambda_{d,i}^t - \lambda_{\gamma,i}^t)M, \tag{5c}$$

$$|H_{e,i}^t - \Theta_{\alpha,i}| \leqslant (2 - \lambda_{d,i}^t - \lambda_{\alpha,i}^t)M, \tag{5d}$$

$$-(1-\lambda_{\phi,i}^t)M \leqslant p_{c,i}^t - k_{AB,i}S_i^t - b_{AB,i} \leqslant (1-\lambda_{\beta,i}^t)M, \tag{5e}$$

$$-(1-\lambda_{\gamma,i}^t)M \leqslant p_{d,i}^t + k_{CD,i}S_i^t + b_{CD,i} \leqslant (1-\lambda_{\alpha,i}^t)M, \tag{5f}$$

$$\lambda_{\phi,i}^t + \lambda_{\beta,i}^t = 1, \ \lambda_{\gamma,i}^t + \lambda_{\alpha,i}^t = 1, \tag{5g}$$

$$\lambda_{c,i}^t, \lambda_{d,i}^t, \lambda_{\phi,i}^t, \lambda_{\beta,i}^t, \lambda_{\gamma,i}^t, \lambda_{\alpha,i}^t \in \mathbb{Z}, \tag{5h}$$

where $\Theta_{\beta,i}$, $\Theta_{\phi,i}$, $\Theta_{\gamma,i}$, and $\Theta_{\alpha,i}$ represent linear equations for hyperplanes β_i, ϕ_i, γ_i, and α_i, respectively, M is a large positive-valued constant, and the pair of binary variables $(\lambda_{c,i}^t, \lambda_{d,i}^t)$ takes the value of $(1,0)$ when the cell is charging and $(0,1)$ when discharging [10]. Furthermore, parameters $k_{AB,i}$, $b_{AB,i}$ and $k_{CD,i}$, $b_{CD,i}$ are fit from cut lines AB and CD, respectively shown in Figs. 2(a) and 2(b), chosen to minimize the difference between the approximate hyperplanes and actual surfaces obtained from the PDE solution. A brief discussion on the approximation error can be found in [11].

B. Voltage Constraints of Battery Cells

The linear approximation for the voltage profile used in [7] without polarization effects may not sufficiently represent charging behaviour in the CC mode near full capacity. We thus develop a more accurate nonlinear model by performing numerical PDE simulation of the electrochemical-thermal-coupled model to obtain the voltage v_i^t of a battery cell in ES_i in time period $t \in \mathcal{T}$ in the CC charging mode. We can then plot the variations in v_i^t with respect to the charging power $p_{c,i}^t$ and SoC S_i^t. As an example, Fig. 3(a) plots one such surface resulting from a simulation over a scheduling horizon of one hour subdivided into time periods of length $\Delta t = 15$ minutes under fixed $T_{\mathrm{amb}} = 27°\mathrm{C} = 300.5\,\mathrm{K}$ along with other battery parameter values reported in [11]. The CC charging mode terminates once v_i^t reaches its maximum allowable limit of $\overline{v}$, shown as a surface in grey colour in Fig. 3(a) with $\overline{v} = 3.65\,\mathrm{V}$. Its intersection with the voltage profile surface is the line EF marked in red colour. Projection of line EF onto the $(S_i^t, p_{c,i}^t)$-plane then yields the following upper bound of the SoC at the maximum voltage limit given a particular charging power:

$$S_i^{t+\Delta t} \leqslant k_{EF,i}p_{c,i}^t + b_{EF,i}, \ 0 \leqslant S_i^t \leqslant 1, \tag{6}$$

where parameters $k_{EF,i}$ and $b_{EF,i}$ are fitted from the projection of line EF, an example of which is shown in Fig. 3(b). Establishing the upper bound in (6) for the worst-case voltage, i.e., its maximum limit, circumvents the need to model the full-blown nonlinear cell voltage profile.

The plots exemplified in Fig. 3 assume that the battery cell can be charged to full SoC in one hour at the nominal charging power of $p^t_{c,i} = 1.10\,\text{kW}$, marked as point F, whereas point E takes a maximum charging power of $p^t_{c,i} = \overline{p}_i = 1.71\,\text{kW}$. Indeed the CC charging mode with $p^t_{c,i} > 1.10\,\text{kW}$ does not fully charge the battery cell before it reaches the maximum allowable voltage, thus limiting applications for long-voyage transportation. As shown in Fig. 3(a), the cell voltage grows exponentially with S^t_i when the SoC is nearly zero or nearly full due to polarization effects in battery charging. Unlike [7] that approximates the voltage profile as a linear function leading to optimal schedules that, when realized, may not charge cells to their full capacity, our approach ensures charging to full capacity. Finally, we note that we replace the cell voltage profiles with a linear constraint of $S^{t+\Delta t}_i$ and $p^t_{c,i}$ in (6), thereby perfectly avoiding the nonlinearity of cell voltage profiles. In addition, discharging a battery at constant current reduces the cell voltage, and the battery reaches zero capacity without voltage limit issues.

C. Problem Formulation

The optimal S2G dispatch seeks to track a specified reference power signal using the combination of ESs and WECS. Suppose that BESSs in N_E ESs are scheduled over N_T time periods to charge and discharge to collectively balance the WECS output p^t_w and track a net-power reference signal p^t_{ref}, $t \in \mathcal{T}$, prescribed by the grid operator. Further suppose the BESS in ES_i comprises $n_{e,i}$ identical battery cells, where decision variables for one such cell consist of S^t_i, $p^t_{c,i}$, $p^t_{d,i}$, $\lambda^t_{c,i}$, $\lambda^t_{d,i}$, T^t_i, $H^t_{e,i}$, $\lambda_{\beta,i}$, $\lambda_{\phi,i}$, $\lambda_{\alpha,i}$, and $\lambda_{\gamma,i}$. We then formulate the optimal S2G dispatch model as follows:

$$\min \; F = \sum_{t=0}^{N_T\Delta t} \left\| p^t_w - \sum_{i=1}^{N_E} n_{e,i}(p^t_{c,i} + p^t_{d,i}) - p^t_{\text{ref}} \right\|_2^2, \quad (7a)$$

$$\text{s.t. } S^{t+\Delta t}_i = S^t_i + \eta_{c,i} p^t_{c,i}\Delta t + \eta_{d,i} p^t_{d,i}\Delta t, \quad (7b)$$

$$0 \leqslant p^t_{c,i} \leqslant \lambda^t_{c,i}\overline{p}_i, \;\; -\lambda^t_{d,i}\overline{p}_i \leqslant p^t_{d,i} \leqslant 0, \;\; \lambda^t_{c,i} + \lambda^t_{d,i} = 1, \quad (7c)$$

$$\text{(4a)–(4e), (5a)–(5h), (6), } \forall\, t \in \mathcal{T}, \;\; S^{N_T\Delta t}_i = 1, \quad (7d)$$

where $\eta_{c,i}$ and $\eta_{d,i}$ respectively denote the charging and discharging efficiency coefficients for the BESS in ES_i, and $\overline{p}_i$ is the maximum charging or discharging power.

III. Numerical Case Studies

We perform optimal S2G dispatch for an offshore floating charging station serving $N_E = 3$ ESs, as shown in Fig. 1, over a 24-hour scheduling horizon beginning at 07:00, subdivided into $N = 96$ time periods of length $\Delta t = 15$ minutes. Our typical desktop computer incurs about 17 minutes to solve the optimal dispatch, well within the scheduling horizon. Suppose each ES has two BESSs, both with initial SoC value S^0 and initial temperature $T^0 = 27°\text{C}$. We set $\overline{T} = 50°\text{C}$, $\eta_{c,i} = \eta_{d,i} = 0.99$ for all cells. Considering standard air conditioning range of 25°C to 30°C, we solve the S2G dispatch for cases with $T_{\text{amb}} = 27°\text{C}$ and $T_{\text{amb}} = 30°\text{C}$. Simulations performed in COMSOL with battery parameter values reported in [11] yield PDE solutions needed to determine parameters $k_{AB,i} = -0.118$ and $b_{AB,i} = 0.118$ in (5e), $k_{CD,i} = 0.3$ and $b_{CD,i} = 0$ in (5f), and $k_{EF,i} = -0.5501$ and $b_{EF,i} = 1.11$ in (6).

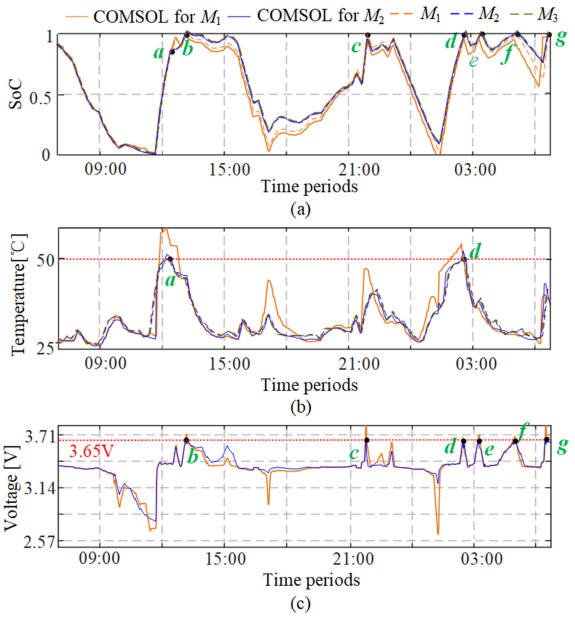

Fig. 4. Optimal S2G dispatch solution for ES_1: (a) SoC, (b) cell temperature, (c) cell voltage.

1) Optimal Solution: Plotted as dashed traces in Fig. 4 are optimal decisions for ES_1 from the method in [10] (M_1) without cell temperature and voltage constraints serving as a benchmark to compare the proposed optimal S2G dispatch incorporating them with $T_{\text{amb}} = 27°\text{C}$ (M_2) and $T_{\text{amb}} = 30°\text{C}$ (M_3). Solid traces in Fig. 4 represent COMSOL PDE solutions given optimal decisions from M_1 or M_2 as inputs.

High charging or discharging powers to balance sharp fluctuations in WECS outputs (points a and d in Fig. 4(a)) lead to large values of $H^t_{e,1}$ that then cause cell temperature T^t_1 to increase rapidly. As shown by corresponding points a and d in Fig. 4(b), M_1 yields decisions that lead to cell temperature violations in the COMSOL simulation during 12:45–13:15 and 02:30–03:00 whereas M_2 closely approximates the realized temperature and limits its value. Furthermore, COMSOL realizations of the SoCs plotted in Fig. 4(a) demonstrate M_2 incorporating voltage constraints charges the BESS to full capacity at all points b to g, unlike M_1. By examining the corresponding points b to g in Fig. 4(c), we conclude that indeed M_1 is unable to charge the BESSs to full capacity having terminated the CC charging mode upon reaching the maximum voltage limit. Finally, we find that modifying T_{amb} from 27°C in M_2 to 30°C in M_3 has negligible impact on the optimal dispatch in Fig. 4(a) and the realized cell temperature in Fig. 4(b). This is because T_{amb} appears in the approximate temperature model in (4a) via the coefficient ω_3 only, the value of which changes by merely 0.9% due to the 3°C difference.

2) Thermal and Voltage Model Accuracy: Using the same parameter settings as those to produce Fig. 2, we plot variations in cell temperature $T^{t+\Delta t}_i$ with respect to S^t_i and $p^t_{c,i}$ yielded by a PDE solver in Fig. 5(a) and compare them to the approximate discretized temperature model in (4a) (yellow and pink colours) and the linear model from [6] (grey colour).

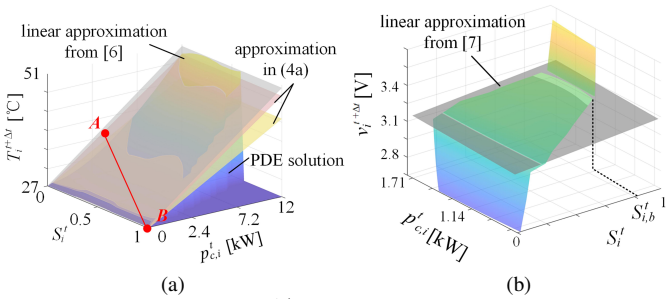

(a) (b)

Fig. 5. (a) Approximating T_i^{t+1} for battery cell charging, (b) Cell voltage surface and linear approximation.

The approximate temperature in yellow colour corresponding to hyperplane β_i in Fig. 2(a) is active below the cut line AB, otherwise that in pink colour corresponding to hyperplane ϕ_i is active. An analogous plot for discharging can be found in [11, Fig. 2]. The cell temperature approximated by (4a) in Fig. 5(a) closely resembles the surface yielded by the PDE solver, with the maximum errors between the two in charging and discharging modes being 1.2°C and 1.8°C, respectively, which are acceptable for the optimal S2G dispatch as demonstrated by numerical case studies in Section III-1. In contrast, the maximum cell temperature errors of the linear model are 5.1°C and 5.9°C for charging and discharging modes, respectively.

In Fig. 5(b), we plot variations in cell voltage with respect to $p_{c,i}^t$ and S_i^t obtained from a PDE solution as compared to the linear model from [7] (grey colour). The linear approximation appears reasonable within a certain range of battery cell operation, but approximation errors grow as SoC increases, especially when $S_i^t \geqslant S_{i,b}^t$. Notably, the constraint formed by the linear approximation being less than $\overline{v}$ is never binding regardless of SoC, leading to potentially infeasible battery dispatch (see, e.g., M_1 in Fig. 4). Also, even if the SoC were enforced to be below $S_{i,b}^t$, the linear cell voltage model still may not be sufficiently accurate for optimal S2G dispatch (see example in [11, Section IV]).

IV. Concluding Remarks

In this letter, we developed an optimal S2G dispatch incorporating thermal and voltage constraints of battery cells based on the electrochemical-thermal-coupled model to enable ESs to provide grid services coupled with onshore or offshore WECS. Numerical case studies demonstrate that realizations of the optimal decisions from the proposed S2G dispatch satisfy battery thermal constraints and lead to fully charged BESS in the fast CC charging mode, thus making ESs effective for long-voyage transport and for smoothing out WECS outputs.

References

[1] R. Li, H. Li, W. Huang, H. Tao, W. Xu, N. Tai, and C. Li, "Accelerating green shipping with spatially optimized offshore charging stations," *Nat. Energy*, 2025.

[2] L. Frković, B. Ćosić, T. Pukšec, and N. Vladimir, "The synergy between the photovoltaic power systems and battery-powered electric ferries in the isolated energy system of an island," *Energy*, 2022.

[3] S. Li, C. Ye, Y. Ding, Y. Song, and M. Bao, "Reliability assessment of renewable power systems considering thermally-induced incidents of large-scale battery energy storage," *IEEE Trans. on Power Systems*, vol. 38, no. 4, pp. 3924–3938, 2023.

[4] V.-B. Vu, D.-H. Tran, and W. Choi, "Implementation of the constant current and constant voltage charge of inductive power transfer systems with the double-sided lcc compensation topology for electric vehicle battery charge applications," *IEEE Trans. on Power Electron.*, vol. 33, no. 9, pp. 7398–7410, 2018.

[5] B. Xu, A. Oudalov, A. Ulbig, G. Andersson, and D. S. Kirschen, "Modeling of lithium-ion battery degradation for cell life assessment," *IEEE Trans. on Smart Grid*, vol. 9, no. 2, pp. 1131–1140, 2018.

[6] Y. Chen, K. Zheng, Y. Gu, J. Wang, and Q. Chen, "Optimal energy dispatch of grid-connected electric vehicle considering lithium battery electrochemical model," *IEEE Trans. on Smart Grid*, vol. 15, no. 3, pp. 3000–3015, 2024.

[7] T. Morstyn, C. Crozier, M. Deakin, and M. D. McCulloch, "Conic optimization for electric vehicle station smart charging with battery voltage constraints," *IEEE Trans. on Transp. Electr.*, vol. 6, no. 2, pp. 478–487, 2020.

[8] H. Ji, T. Luo, L. Dai, Z. He, and Q. Wang, "Numerical investigation on the polarization and thermal characteristics of $LiFePO_4$-based batteries during charging process," *Appl. Therm. Eng.*, vol. 214, p. 118709, 2022.

[9] Y. Gao, X. Zhang, B. Guo, C. Zhu, J. Wiedemann, L. Wang, and J. Cao, "Health-aware multiobjective optimal charging strategy with coupled electrochemical-thermal-aging model for lithium-ion battery," *IEEE Trans. on Ind. Inform.*, vol. 16, no. 5, pp. 3417–3429, 2020.

[10] D. Pozo, "Convex hull formulations for linear modeling of energy storage systems," *IEEE Trans. on Power Syst.*, vol. 38, no. 6, pp. 5934–5936, 2023.

[11] C. Lei, S. Li, and Y. C. Chen. Supplementary material for "optimal ship-to-grid dispatch considering battery thermal and voltage electrochemical-thermal-coupled constraints". [Online]. Available: https://github.com/honolulufishing/supplementary_material/blob/main/ieee_supple_S2G.pdf